Experimental Investigation of Molten Salt Droplet Quenching and Solidification Processes of Heat Recovery in Thermochemical Hydrogen Production

S. Ghandehariun[1], Z. Wang[2], G. F. Naterer[3], M. A. Rosen[2]
[1]Faculty of Engineering, University of Alberta
[2]Faculty of Engineering and Applied Science, University of Ontario Institute of Technology
[3]Faculty of Engineering and Applied Science, Memorial university of Newfoundland
Email: samane@ualberta.ca

Abstract

This paper investigates the heat transfer and x-ray diffraction patterns of solidified molten salt droplets in heat recovery processes of a thermochemical Cu-Cl cycle of hydrogen production. It is essential to recover the heat of the molten salt to enhance the overall thermal efficiency of the copper-chlorine cycle. A major portion of heat recovery within the cycle can be achieved by cooling and solidifying the molten salt exiting an oxygen reactor. Heat recovery from the molten salt is achieved by dispersing the molten stream into droplets. In this paper, an analytical study and experimental investigation of the thermal phenomena of a falling droplet quenched into water is presented, involving the droplet surface temperature during descent and resulting composition change in the quench process. The results show that it is feasible to quench the molten salt droplets for an efficient heat recovery process without introducing any material imbalance for the overall cycle integration.

Keywords: hydrogen production; thermochemical water splitting; heat recovery; molten salt

1. Introduction

Worldwide energy demand is increasing rapidly due to the continuing increase in world population and the desires of developing countries to improve their living standards. A large portion of the world energy demand is met by fossil fuels, because of their availability and convenience. However, it is expected that fossil fuel production worldwide may peak in about 15 years and thereafter begin to decrease [1]. Also, the environmental damage caused by fossil fuel usage and their combustion products is a major problem [2, 3]. Hydrogen is a potentially major solution to the problems of climate change. It burns cleanly to produce water without emissions. It is used in fuel cells to generate electricity directly. Its energy content per unit

30   mass is 2.5 times higher than that of any other conventional fuels [3, 4]. Therefore, hydrogen is a promising

31   energy carrier and storage medium for renewable energy resources [3-7]. Lu et al. [8] analyzed the

32   feasibility of an optimal cascade hydropower system using hydrogen, produced from water electrolysis, as

33   an energy storage medium. The authors showed that by using hydrogen production and storage in

34   hydropower stations, more water resources can be used for electricity and hydrogen production, hence the

35   amount of unused water is reduced and electricity generation reliability (EGR) is improved [8]. The

36   economic viability of hydrogen production and storage from excess electricity in a 50 MW wind power

37   plant was investigated by Kroniger and Madlener [9]. Their results showed that the power-to-fuel plant

38   could be operated profitably at a hydrogen price of over 0.36 €/m^3 with 100% utilization of the electrolyzer

39   if the hydrogen is directly marketed instead of using it to store and re-generate electrical energy [9]. Coupled

40   operation of a wind turbine and electrolyzer was investigated by Sarrias-Mena et al. [10]. The authors

41   evaluated four different electrolyzer configurations under variable wind speeds and grid demand.

42   Most of the hydrogen currently produced in the world is derived from fossil fuels through different

43   types of reforming processes [11, 12]. Developing a sustainable, large-scale, low-cost method of hydrogen

44   production from energy sources other than fossil fuels is required to reduce GHG emissions and accelerate

45   the transition to a clean future. Water electrolysis and thermochemical cycles, using various heat sources,

46   are alternative methods for sustainable hydrogen generation [13-15]. Han et al. [16] reported the effect of

47   various operating conditions and design parameters on the performance of proton exchange membrane

48   (PEM) electrolyzer cells. Their results show that PEM electrolyzer cell performance improves with a

49   decrease in electrode thickness and membrane thickness due to lower diffusion overpotential and ohmic

50   losses. At a current density of 1.5 A/cm^2, the performance loss due to the interfacial resistance between the

51   electrode and the membrane contributes 31.8% of the total ohmic loss. An experimental study on hydrogen

52   production from a 200 W solid oxide stack working in a reverse mode was presented by Penchini et al. [17].

53   The influence of steam dilution, water utilization and operating temperature on conversion efficiency and

54   the stack's thermal balance was evaluated. The tests were performed at three different operating

55 temperatures over a range of steam inlet concentrations from 50% to 90% and water utilization up to 70%.

56 The net flows up to 2.4 ml/(min cm^2) of hydrogen and 1.2 ml/(min cm^2) of oxygen were measured [17].

57 A thermochemical cycle has a potentially higher overall efficiency compared to water electrolysis

58 as heat is used directly to generate hydrogen to avoid the thermal energy losses in the heat-to-electricity

59 conversion process. Water electrolysis has an overall heat-to-hydrogen efficiency of about 24%, based on

60 the higher heat value of hydrogen, while thermochemical cycles can reach a heat-to-hydrogen efficiency

61 up to about 50% [18].

62 A thermochemical water splitting process includes decomposition of water into oxygen and

63 hydrogen using only heat in a fully thermochemical cycle, or a combination of electricity and heat in a

64 hybrid cycle. The net reaction is as follows:

$$H_2O(l) \rightarrow H_2(g) + 1/2 \ O_2(g) \tag{1}$$
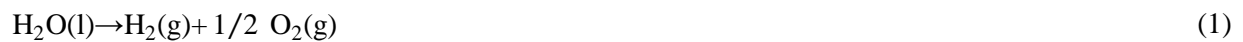
65 Several thermochemical water splitting cycles, using various sources of energy, have been studied

66 in the past [19-23]. The sulfur-iodine thermochemical cycle, in which solar energy is used for the

67 decomposition of sulphuric acid, was investigated by Huang and Raissi [24]. Xinxin and Kaoru [25] studied

68 the sulfur-iodine (S-I) cycle for hydrogen production using nuclear energy. Energy and economic

69 assessment of an industrial plant for hydrogen production by a sulfur-iodine thermochemical cycle was

70 presented by Liberatore et al. [26]. The efficiency of the thermochemical cycle by itself was about 34%,

71 based on the higher heat value. If this value is associated with the electrical energy production, including

72 the efficiency of the solar plants, the total heat-to-hydrogen efficiency was obtained to be 21%. Varsano et

73 al. [27] analyzed a sodium manganese mixed ferrite thermochemical cycle with a solar reactor receiver

74 packed with pellets of a reactive mixture to investigate the feasibility of the process. The temperature at

75 which the reactor operates is nearly constant within the range of 700-800ºC. About 130-460 micromole

76 hydrogen per gram of mixture is produced during one hour operation of the reactor. An iron-chlorine

77 thermochemical cycle was studied by Canavesio et al. [28]. The theoretical and experimental study was

78 carried out at a laboratory scale to investigate the reaction pathway and the kinetics of the thermochemical

79 cycle in order to improve its overall performance in terms of energy efficiency and hydrogen yield. Xu and

3

80   Wiesner [29] presented a conceptual design of a two-step iron oxide cycle for production of hydrogen.

81   Molten FeO is used as a storage and heat transfer medium. After five days, the hydrogen production was

82   stabilized at 7 kg/min.

83   Alternative thermochemical cycles of hydrogen production were evaluated by Lewis et al. [30-32].

84   Their results showed that the copper-chlorine cycle is chemically possible and feasible concerning

85   engineering aspects and energy efficiency. Dincer and Balta [33] have discussed several cycles for

86   hydrogen production from nuclear energy. The Cu-Cl thermochemical cycle was shown a promising cycle

87   for nuclear-based hydrogen production. Recent advances in thermochemical cycles of hydrogen production,

88   using non-fossil energy sources such as nuclear or solar, were reported by Rosen [18]. The copper-chlorine

89   cycle was shown to have significant potential because of the lower temperature requirement for heat

90   supplies compared to most other thermochemical cycles. It is necessary to improve the overall thermal

91   efficiency of the Cu-Cl hydrogen production method. Therefore, heat recovery within the cycle is an

92   essential part of the process. This paper investigates a direct contact heat recovery process in the copper-

93   chlorine cycle of hydrogen production.

94

95   **2. Copper-chlorine Cycle for Hydrogen Production**

96   The copper-chlorine cycle decomposes water into oxygen and hydrogen, through intermediate copper and

97   chloride compounds, in a closed loop in which all chemicals are recycled continuously. There are three

98   variations of the Cu-Cl cycle, based on the number of main chemical reactions: three steps, four steps, and

99   five steps. The schematic of the four step cycle is shown in Fig. 1.

100   The first step in the four-step cycle Cu-Cl thermochemical cycle for hydrogen production is

101   CuCl/HCl electrolysis:

$$2CuCl(aq)+2HCl(aq)\rightarrow H_2(g)+2CuCl_2(aq) \tag{2}$$

102   where oxidation of copper(I) chloride takes place during an electrochemical reaction, in the presence of

103   hydrochloric acid to produce copper(II) chloride and hydrogen.

104   The second step of the Cu-Cl cycle is drying in which aqueous $CuCl_2$ exiting the electrolysis step

105   is dried to produce solid $CuCl_2$ particles:

$$CuCl_2(aq) \rightarrow CuCl_2(s) \tag{3}$$

106   The $CuCl_2$ particles are then moved to the third step which is hydrolysis, and reacted with superheated

107   steam to perform copper oxychloride hydrochloric HCl and Cu_2OCl_2:

$$2CuCl_2(s) + H_2O(g) \rightarrow Cu_2OCl_2(s) + 2HCl(g) \tag{4}$$

108   Step 4 is the oxygen production step where solid particles of copper oxychloride decompose into

109   molten copper(I) chloride and oxygen:

$$Cu_2OCl_2(s) \rightarrow 2CuCl(l) + 1/2\,O_2(g) \tag{5}$$

110   Several variations of copper-chlorine cycles with different numbers of steps and methods of grouping were

111   compared, and major features of the cycles with different numbers of steps were discussed by Wang et al.

112   [34]. A detailed kinetic study of the hydrogen and oxygen production reactions in the Cu-Cl cycle was

113   presented by Serban et al. [35]. Canadian advances in nuclear-based production of hydrogen by the Cu-Cl

114   cycle were presented by Naterer et al. [36-39]. Thermophysical properties of copper compounds in the Cu-

115   Cl cycle were studied by Zamfirescu et al. [40]. The environmental impacts of the Cu-Cl cycle were

116   presented by Ozbilen et al. [41] using life cycle assessment.

117   Hydrolysis of $CuCl_2$ into Cu_2OCl_2 and HCl using a spray reactor was investigated by Ferrandon

118   et al. [42]. It was shown that a counter-current flow reactor results in a significantly higher yield of Cu_2OCl_2

119   compared to a co-current flow, due to enhanced mass transfer. Naterer et al. [43] examined the evaporative

120   drying of aqueous copper(II) chloride $CuCl_2$ droplets in the copper-chlorine cycle. The results showed that

121   benefits of flashing the solution to enhance drying were relatively minor, compared to evaporative drying

122   in the spray drying process.

123

124   **3. Heat Recovery for Thermal Integration of the Cu-Cl Cycle**

125   Regardless of the variations of the Cu-Cl cycles, molten salt of CuCl is produced in the oxygen production

126   step, and aqueous CuCl (i.e. CuCl dissolved in the hydrochloric acid) is used in the hydrogen production

127 step as a reactant. This means that the solidification, dissolution, and heat recovery of CuCl commonly exist

128 in all types of Cu-Cl cycles linking the oxygen and hydrogen production steps. The processing of CuCl will

129 significantly affects the efficiency of the copper-chlorine cycle and the complexity of the process

130 integration from the perspectives of the integration of thermal energy and material flows. This paper will

131 examine the fundamental phenomena in the molten salt thermal energy recovery process, and the influence

132 of the heat recovery method on the integration of material flows.

133   Heat recovery within the copper-chlorine cycle is crucial to the efficient performance and the

134 overall viability of the cycle [36-39]. The heat requirements of different steps of the five-step copper-

135 chlorine cycle were evaluated by Naterer et al. [44]. The authors evaluated the heat matching between the

136 steps of the copper-chlorine cycle so as to recover as much heat as feasible and minimize the net heat

137 requirement of the Cu-Cl cycle. It was shown that the thermal efficiency of the Cu-Cl cycle improves

138 significantly if all the heat released is recovered in the cycle [44].

139   Thermal analysis of the four-step Cu-Cl cycle was performed by Ghandehariun et al. [45]. A pinch

140 analysis was used to determine how much heat can be recovered within the cycle, and where in the cycle

141 the recovered heat can be used. About 18% of the total required heat of the copper-chlorine cycle can be

142 obtained by cooling HCl, O_2, and molten CuCl. About 88% of the total heat recovery can be achieved by

143 cooling molten CuCl exiting the oxygen reactor step of the cycle at about 530ºC. Therefore, the focus of

144 heat recovery is on heat recovery from molten CuCl. Since the melting point of CuCl is about 430ºC,

145 solidification occurs as molten CuCl cools. A comparison of various processes for heat recovery from

146 molten copper (I) chloride was explored by Ghandehariun et al. [46]. It was shown that a portion of heat

147 recovery can be used to produce superheated steam required for the hydrolysis step of the cycle. However,

148 the remainder can be used only in the drying step due to its lower temperature [46].

149   Two types of heat recovery methods can be considered: indirect and direct contact. In an indirect

150 contact heat transfer equipment such as a shell and tube heat exchanger, molten CuCl flows through an

151 inner pipe while the coolant flows through the outer pipe [47]. In a direct contact heat recovery process,

152 molten CuCl can be first dispersed into droplets that subsequently fall down to a water bath for quenching,

153 and at the same time the generated steam flows upwards to form a counter current contact with the falling

154 droplets. The droplets are cooled and solidified during the descent and quench. Heat transfer from the

155 droplet occurs by three main mechanisms: convection heat transfer, mass transfer, and radiation heat

156 transfer.

157 The selection of the heat recovery methods are restricted by the material integration of the Cu-Cl

158 cycle. As presented previously, instead of the molten CuCl, the solidified CuCl is used in the downstream

159 electrolysis step. This suggests that the shell and tube heat recovery system may not be preferable, because

160 the solidification is not desirable inside the tube or shell. The processing of solidified CuCl in a shell and

161 tube heat exchanger is very challenging. Direct contact with a water quench was selected as the heat

162 recovery method in this paper. The CuCl exiting the heat recovery system (i.e. solidified CuCl) is used in

163 another part of the cycle (i.e. electrolysis step). Therefore, it is essential to avoid any possible undesirable

164 chemical reactions during the direct quench process. In addition to obtaining fundamental heat transfer data,

165 this paper will also investigate the feasibility of using the direct quench process from a chemical

166 composition perspective.

167

168 **4. Heat Transfer Formulation**

169 The velocity of a falling droplet is evaluated by solving Newton's second law of motion for a freely-falling

170 droplet as follows:

$$m_d \left(\frac{dv}{dt} \right) = m_d g \left(1 - \frac{\rho_g}{\rho_d} \right) - \frac{1}{8} \pi d^2 \rho_g C_D v^2 \qquad (6)$$

171 where C_D is the drag coefficient and calculated from the following correlation over $Re < 3 \times 10^5$ [48].

$$C_D = \frac{24}{Re} (1 + 0.15 Re^{0.687}) + \frac{0.42}{1 + 4.25 \times 10^4 Re^{-1.16}} \qquad (7)$$

172 The temperature profile in the droplet is assumed to be uniform and resistance to heat transfer exists only

173 in the surrounding gas. The rate of temperature change is modeled by a heat balance between the droplet

174 and the surrounding gas:

$$m_d c_{p,d} \frac{dT_d}{dt} = -\dot{q}_c \tag{8}$$

175 where $\dot{q}_c$ represents convective heat transfer from the droplet surface. It can be expressed as:

$$\dot{q}_c = h_c A(T_d - T_\infty) \tag{9}$$

176 where h_c is the convection heat transfer coefficient, A is the droplet surface area, and T_d and T_∞ are the

177 droplet and ambient gas temperatures, respectively. The convection heat transfer coefficient is found by:

$$h_c = \frac{Nu\, k_g}{d} \tag{10}$$

178 where Nu is the Nusselt number, k_g is the thermal conductivity of the ambient gas, and d is the diameter of

179 the droplet.

180   The Nusselt number is calculated by the following correlation of Ranz and Marshall [49] for freely

181 falling liquid drops:

$$Nu = 2 + 0.6 Re^{\frac{1}{2}} Pr^{\frac{1}{3}} \tag{11}$$

182 where Re is the Reynolds number and Pr is the Prandtl number. Solving the above equations with the initial

183 condition $T_d(0) = T_i$ yields:

$$\frac{T_d - T_\infty}{T_i - T_\infty} = \exp(-\frac{h_c A}{m_d c_{p,d}} t) \tag{12}$$

184

185 **4. Experimental Study**

186 **4.1 Apparatus and Procedure**

187 The purity of CuCl in the experiments is 99.9%. The melting point is 420ºC. In the experiments, solid

188 powder of CuCl was placed into an inclined pipe and heated to melt CuCl inside the pipe. The CuCl flowed

189 out and formed molten salt droplets. In addition to using the inclined pipe to generate molten droplets, a

190 heating mantle was also used to produce molten CuCl and then molten salt was poured into a small container

191 with a nozzle at the bottom. The nozzle diameter was changed so that different droplet diameters could be

192 obtained. The molten droplets exiting the nozzle fell through air and eventually into a water vessel. The

8

193   distance of the droplet in air was about 80 cm. The surface temperature of the droplet during the flight was

194   measured by a Flir SC5600 infrared camera.

195   The droplets fell through the air and then released heat into a vessel of water. The water depth in

196   the quench cell was 25 cm, and the descent distance from the pipe exit to the water level could be adjusted

197   in the range of 60-120cm. An infrared thermal imaging system was used to measure the temperature of the

198   droplets during the descent. At the same time, a visible light camera was used to record the shape and

199   quench phenomena of the droplets.

200   To investigate the possible reactions between copper(I) chloride and water or air, two sets of

201   experiments were performed. In one set of experiments, the solidified product in water was collected and

202   dried in air. In the other set of experiments, the solidified material was kept in a small container filled with

203   water, in a nitrogen glove box, to avoid exposure to air. The composition of each prepared sample was then

204   determined by an X-ray diffractometer to examine the existence of undesirable chemical reactions during

205   the quench process. The experiments were implemented in a fume enclosure to avoid the risk of CuCl

206   hazards.

207

208   **4.2 Temperature measurements**

209   An infrared (IR) imaging technique was used in the experiments to measure the surface temperature of a

210   droplet. An infrared camera receives radiation from surroundings and the target object. Both of these

211   radiation components become attenuated passing through the atmosphere. The atmosphere itself also

212   radiates some energy, which causes the background temperature in the readings of the infrared camera. The

213   total radiation received by the infrared camera is espressed as:

$$W = W_1 + W_2 + W_3 \tag{13}$$

214   where W_1 is the energy received due to emission from the object, given by:

$$W_1 = \tau \, \epsilon \, E_b(T_{obj}) \tag{14}$$

215   Here, ε is the emissivity of the object, τ is the transmittance of the atmosphere, and $E_b(T_{obj})$ is the

216   blackbody emission at the object temperature. Also, W_2 is the energy received due to the reflected emission

217   from surrounding sources, given by:

$$W_2 = \tau\,(1 - \epsilon)\,E_b(T_{sur}) \tag{15}$$

218   where (1-ε) is the reflectivity of the object. Also, W_3 is the emission from the atmosphere, given by:

$$W_3 = (1 - \tau)\,E_b(T_{atm}) \tag{16}$$

219   where (1-τ) is the emissivity of the atmosphere. To calculate the correct target object, the IR camera

220   software needs inputs for the atmospheric temperature and attenuation, emissivity of the object, and the

221   surrounding temperature. These parameters can be assumed, measured, or obtained from tables.

222   To obtain an accurate value of the emissivity of the molten CuCl in the temperature range of

223   interest, an infrared camera (OPTRIS PI160) was calibrated with a type K thermocouple to measure the

224   temperature of molten salt contained in a vessel of 15 cm diameter. The specifications of the infrared camera

225   are listed in Table 1. The type K thermocouple was integrated with a Labview data acquisition system

226   which could measure a voltage range of ±80 mv for the temperature range of 30-1000 °C. The uncertainty

227   of the output of the type K thermocouple was ±0.1% of the span, which is equivalent to ±0.97 °C. In the

228   emissivity calibration experiments, the molten salt in the vessel was about 1 cm thick to have good mixing,

229   and the thermocouple was placed 0.5 cm below the molten salt surface level.

230   As the infrared camera can measure the surface temperature, the molten salt immediately

231   surrounding the thermocouple was agitated to refresh the surface and make the surface temperature the

232   same as the temperature at 0.5cm below the surface. The infrared camera was calibrated based on the

233   thermocouple reading. The CuCl existed simultaneously in both liquid and solid forms, several centimetres

234   from the thermocouple at the molten CuCl surface, because the surface was cooled down to its solid phase

235   to form a very thin solid layer on the molten salt surface. These co-existing two phases should give a

236   temperature reading of the melting point, 420°C. In the experiment, the reading by the calibrated camera

237   was 421°C, which lies in the range of measurement uncertainty. So it is believed that the emissivity

238   determination is valid. One of the infrared images indicated the two-phase surface temperature. The

239   temperature immediately adjacent to the thermocouple is presented in Fig. 2.

240   To measure the droplet temperature, the room temperature was controlled at 21 ℃ in each

241   experiment. As the droplet size is much smaller than the bulk molten stream, a high resolution thermal

242   imaging camera (Flir SC5600 camera) with Altair software was used for thermography of the molten

243   copper(I) chloride droplets. The technical specifications of the IR camera are shown in Table 2. The descent

244   of a droplet was tracked and compared with the thermal images. A visible light camera was used to record

245   the droplet during its descent in the gas stream and quenching at the water surface.

246

247   **4.3 X-ray diffraction system**

248   X-ray diffraction (XRD) was used to examine the composition change in the quench process. XRD is a

249   versatile, non-destructive technique that reveals detailed information about the chemical composition of

250   materials. When X-rays are incident on an atom of the droplet, they make the electron cloud move. The

251   movement of these charges re-radiates the waves with the same frequency. This phenomenon is known as

252   Rayleigh scattering. These re-emitted wave fields interfere with each other, either constructively or

253   destructively, producing a diffraction pattern on the detector. The resulting wave interference pattern creates

254   a Bragg diffraction. The interference is constructive when the phase shift is a multiple of 2π. This condition

255   can be expressed by Bragg's law [50]:

$$n\lambda = 2d\sin\theta \tag{17}$$

256   where n is an integer, λ is the wavelength of the incident wave, d is the spacing between the planes in the

257   atomic lattice, and θ is the angle between the incident ray and the scattering planes.

258   Each crystalline material has a particular X-ray diffraction pattern. The number of peaks observed

259   is related to the symmetry of the unit cell. A unit cell with a higher symmetry has fewer diffraction peaks.

260   The spacings of the observed diffraction peaks are attributed to the repeat distances between planes of atoms

261   in the structure. The intensities of the peaks are identified with the types of atoms in the planes. The

262   scattering intensities for X-rays are related to the number of electrons in the atom. Heavy atoms scatter X-

11

263   rays more effectively than light atoms. As stated earlier, three factors of an X-ray diffraction pattern (i.e.,

264   the number of peaks, positions of the peaks, and the intensities of the peaks) describe a unique X-ray pattern

265   for each substance.

266   A Philips XRD system was used. The basic components of the system are a PW 1830 HT generator,

267   a PW 1050 goniometer, PW 3710 control electronics, and X-Pert system software. During data collection,

268   the sample remains in a fixed situation and the X-ray source and detector are programmed to scan over a

269   range of 2θ values. Here, 2θ is the sum of the angle between the X-ray source and the sample and that

270   between the sample and the detector. Routinely, a 2θ range of $2°$ to $60°$ is acceptable to cover the most

271   useful part of the pattern. An appropriate scanning speed is selected based on a reasonable signal-to-noise

272   ratio for the diffraction peaks.

273   **6. Results and Discussion**

274   From the experiments, it was found that the molten stream at the tube exit breaks into several lumps of

275   irregular shapes, as shown in Figs. 3 and 4. The nozzle type droplet generation device was used to create

276   droplets with a more regular shape. Figure 5 shows the thermal image of a falling droplet using FLIR

277   SC5600. Each image was recorded per 0.01 second and the images were combined to form the full tracking

278   record.

279   Figure 6 shows the surface temperature of a near spherical droplet versus the flight time based on

280   the thermal images in Fig. 5. The droplets fall in ambient air at 21°C. The initial temperature of the droplets

281   is about 504°C. The experimental results represent the maximum temperature of the surface measured by

282   the infrared camera. Since the surface temperature is not uniform, and the droplet rotates during the flight,

283   the maximum surface temperature fluctuates during the flight. However, the maximum surface temperature

284   decreases in 0.11 s. The analytical results are obtained from Eq. (12). The maximum difference between

285   the analytical and experimental results is less than 2%. Figure 6 also shows that the droplet is not solidified

286   in the gas stream if the falling time is insufficient. This result was verified by the visible light-based camera.

287   Figure 7 shows the thermal quench process of a droplet entering the water. The process includes

288 impacting the water surface and forming steam bubbles, breaking of the bubbles, steam generation, and the

289 disintegration of the droplet into many small pieces. It is believed that the small pieces were generated from

290 the evaporation of water and the droplet crust collapse at the interface of water and molten droplets. All

291 droplets disintegrated into small flakes of solid CuCl, even as the descent distance was 95 cm (see Fig. 8).

292   The quench phenomena suggests the avoidance of granulation processes for the solidified CuCl,

293 which is advantageous to the system integration of the oxygen production step, molten salt heat recovery

294 process, and the hydrogen production step in the Cu-Cl cycle. However, the steam generation and the

295 droplet disintegration process may cause a steam explosion if a large amount of molten CuCl is introduced

296 into water.

297   Copper(I) compounds may be unstable in contact with air or water. The possible chemical reactions

298 between copper(I) chloride and water or air were examined. At a temperature of less than 750ºC, the

299 following reaction can occur:

$$2CuCl + \frac{1}{2}O_2 \rightarrow Cu_2O + Cl_2 \tag{18}$$

300 As the atmosphere contains moisture, the following reaction may occur:

$$4CuCl + \frac{3}{2}O_2 + 3H_2O \rightarrow 2Cu_2(OH)_3Cl + Cl_2 \tag{19}$$

301 The copper(I) chloride may also react with water in the presence of oxygen as follows:

$$6CuCl + \frac{3}{2}O_2 + 7H_2O \rightarrow 2Cu_2(OH)_3Cl + 2[CuCl_2.2H_2O] \tag{20}$$
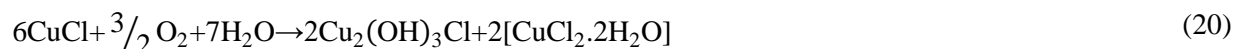
302 As stated earlier, two sets of experiments were performed at different conditions. In the first set of

303 experiments, the solidified CuCl was taken from the water vessel and exposed to air (Fig. 9). The color of

304 the material changes from gray to green. Figures 10 and 11 show the x-ray diffraction results for two

305 experiments. As expected, $Cu_2(OH)_3Cl$ and $CuCl_2.2H_2O$ are observed.

306   In the second set of experiments, solidified CuCl is kept in water in a small container, in a nitrogen

307 glove box. Therefore, the material is not in contact with oxygen. In this case, the color of the material

308 remains gray. The x-ray diffraction results are presented in Figures 12 and 13 for two experiments. It is

309   observed that copper(I) chloride does not react with water in the absence of oxygen. It is also concluded

310   that the molten droplets of CuCl do not react with air during the droplet descent. It is believed that this

311   occurs because the contact time between the droplets and air is very small. For a large industrial scale

312   quench process, it is suggested to drop molten CuCl droplets into water in an inert atmosphere to avoid

313   chemical reactions. Also, the water might be deoxygenated.

314   The uncertainty (U) of the experimental results is determined by [51]:

$$U = \sqrt{B^2 + P^2} \tag{21}$$

315   where B and P represent the bias and precision errors, respectively. The bias error in temperature

316   measurement by the thermal imaging system is ±0.01. The precision error is double the standard deviation

317   of the measured data. A sample of 30 measurements was considered, and the precision error was calculated

318   as ±0.02. The measurement uncertainty was then determined as ±0.02.

319

8. Conclusions

321   Hydrogen can be used as an energy carrier and storage medium along with renewable energy resources.

322   Among various methods of hydrogen production, the copper-chlorine thermochemical cycle has been shown

323   to be a promising method for production of hydrogen due to its lower temperature requirement for heat

324   supply compared to other thermochemical cycles. However, it is essential to improve the overall thermal

325   efficiency of the cycle by effectively recovering heat within the cycle and reducing the net heat requirement

326   of the cycle. Molten salt exiting the oxygen production step of the cycle has a temperature of about 530°C.

327   Heat recovered from cooling and solidifying of molten CuCl may be used to produce superheated steam

328   required in the hydrolysis step of the cycle.

329   In this paper, a direct contact process for heat recovery from molten salt in the Cu-Cl cycle of

330   hydrogen production was studied experimentally and analytically. The molten droplets exiting the nozzle fall

331   through air and eventually quenched into a water vessel. The surface temperature of the droplet during the

332   flight was measured by an infrared camera. The fundamental phenomena such as droplet surface

333 temperature during descent, breaking of molten droplets in water, and the composition change in the quench

334 process were presented. The potential reactions between copper(I) chloride and water or air were

335 investigated through the experiments. The results show that CuCl does not react with water in the absence

336 of oxygen. Therefore, a direct contact process is feasible for recovering heat from molten CuCl in the

337 copper-chlorine cycle. It is feasible to quench the molten salt droplets for an efficient heat recovery process

338 without introducing any material imbalance in the process integration.

339

346

347 **Nomenclature**

A Surface area [m^2]

B Bias

C_D Drag coefficient

c_p Specific heat at constant pressure [J/kg.K]

d Droplet diameter [mm]

E_b Blackbody emissivity power [W]

g Gravitational acceleration [m/s^2]

h_c Convection heat transfer coefficient [$W/m^2 \cdot K$]

k Thermal conductivity [W/m.K]

m Mass [kg]

Nu	Nusselt number
P	Precision
Pr	Prandtl number
$\dot{q}_c$	Convective heat transfer rate [W]
Re	Reynolds number
T	Temperature [°C]
t	Time [s]
U	Uncertainty
v	Velocity [m/s]

348 **Greek symbols**

α	Thermal diffusivity [m^2/s]
β	Fixed (bias) error
δ_k	Measurement error
ϵ	Emissivity
θ	Angle between the incident ray and the scattering planes [rad]
λ	Wavelength of the incident wave [m]
ρ	Density [kg/m^3]

349 **Subscripts**

atm	Atmosphere
d	Droplet
g	Gas
obj	Object
s	Surface
sur	Surroundings
∞	Ambient

350   **References**

351   [1] T. N. Veziroglu, S. Sahin, "21st century's energy", *Energy Conversion and Management*, Vol.

352   49, pp. 1820-1831, 2008.

353   [2] R. L. Nersesian, Energy for the 21st century: A comprehensive guide to conventional and alternative

354   sources, Second Edition. M. E. Sharpe, Armonk, NY, 2010.

355   [3] A. F. Ghoniem, "Needs, resources and climate change: Clean and efficient conversion technologies",

356   *Progress in Energy and Combustion Science*, Vol. 37, pp. 15-51, 2011.

357   [4] P. Ekins, Hydrogen energy: economic and social challenges, Earthscan, London, UK, 2010.

358   [5] K. Christopher, R. Dimitrios, "A review on exergy comparison of hydrogen production methods from

359   renewable energy sources", *Energy and Environmental Science*, Vol. 5, pp. 6640-6651, 2012.

360   [6] A. Midilli, I. Dincer, "Hydrogen as a renewable and sustainable solution in reducing global fossil fuel

361   consumption", *International Journal of Hydrogen Energy*, Vol. 33, pp. 4209-4222, 2008.

362   [7] J. G. G. Clua, R. J. Mantz, H. De Battista"Evaluation of hydrogen production capabilities of a grid-

363   assisted wind-H$_2$ system", *Applied Energy*, Vol. 88, pp. 1857-1863, 2011.

364   [8] D. Lu, B. Wang, Y. Wang, H. Zhou, Q. Liang, Y. Peng, T. Roskilly "Optimal operation of cascade

365   hydropower stations using hydrogen as storage medium", *Applied Energy*, Vol. 137, pp. 56-63, 2015.

366   [9] D. Kroniger, R. Madlener "Hydrogen storage for wind parks: A real options evaluation for an optimal

367   investment in more flexibility", *Applied Energy*, Vol. 136, pp. 931-946, 2014.

368   [10] R. Sarrias-Mena, L. M. Fernandez-Ramirez, C. A. Garcia-Vazquez, F. Jurado "Electrolyzer models

369   for hydrogen production from wind energy systems", *International Journal of Hydrogen Energy*, Vol. 40,

370   pp. 2927-2938, 2015.

371   [11] R. Dell, Clean energy. Royal Society of Chemistry. London, UK, 2004.

372   [12] R. Kothari, D. Buddhiand, R. L. Sawhney, "Comparison of environmental and economic aspects of

373   various hydrogen production methods", *Renewable and Sustainable Energy Reviews*, Vol. 12, pp. 553-563,

374   2008.

17

375 [13] H. Li, G. Tan, W. Zhang, S. Suppiah, "Development of direct resistive heating method for SO_3

376 decomposition in the S-I cycle for hydrogen production", *Applied Energy*, Vol. 93, pp. 59-64, 2012.

377 [14] S. Ghandehariun, G. F. Naterer, I. Dincer, M. A. Rosen, "Solar thermochemical plant analysis for

378 hydrogen production with the copper-chlorine cycle", *International Journal of Hydrogen Energy*, Vol. 35,

379 pp. 8511-8520, 2010.

380 [15] B. S. Kwak, J. Chae, M. Kang, "Design of a photochemical water electrolysis system based on a W-

381 typed dye-sensitized serial solar module for high hydrogen production", *Applied Energy*, Vol. 125, pp. 189-

382 196, 2014.

383 [16] B. Han, S. M. Steen III, J. Mo, F. Zhang "Electrochemical performance modeling of a proton exchange

384 membrane electrolyzer cell for hydrogen energy", *International Journal of Hydrogen Energy*, Vol. 40, pp.

385 7006-7016, 2015.

386 [17] D. Penchini, G. Cinti, G. Discepoli, U. Desideri "Theoretical study and performance evaluation of

387 hydrogen production by 200 W solid oxide electrolyzer stack", *International Journal of Hydrogen Energy*,

388 Vol. 39, pp. 9457-9466, 2014.

389 [18] M. A. Rosen, "Advances in hydrogen production by thermochemical water decomposition: A review",

390 *Energy*, Vol. 35, pp. 1068-1076, 2010.

391 [19] Y. Zhang, H. Yang, J. Zhou, Z. Wang, J. Liu, K. Cen, "Detailed kinetic modeling of homogeneous

392 H_2SO_4 decomposition in the sulfur-iodine cycle for hydrogen production", *Applied Energy*, Vol. 130, pp.

393 396-402, 2014.

394 [20] S. Ghandehariun, Z. Wang, M. A. Rosen, G. F. Naterer, "Reduction of hazards from copper (I) chloride

395 in a Cu-Cl thermochemical hydrogen production plant", *Journal of Hazardous Materials*, Vol. 229-230,

396 pp. 48-56, 2012.

397 [21] L. Roca, A. de la Calle, L. J. Yebra, "Heliostat-field gain-scheduling control applied to a two-step
398 solar hydrogen production plant", *Applied Energy*, Vol. 103, pp. 298-305, 2013.

399 [22] X. Zhang, H. Jin, "Thermodynamic analysis of chemical-looping hydrogen generation", *Applied*
400 *Energy*, Vol. 112, pp. 800-807, 2013.

[23] S. Ghandehariun, M. Talimi, G. F. Naterer, M. A. Rosen, "Analysis of the hazards for the molten cuprous chloride pouring operation in an industrial hydrogen production facility", *Int. J. of Energy Research,* Vol. 37, pp. 358-369, 2013.

[24] C. Huang, A. T. Raissi, "Analysis of sulfure iodine thermochemical cycle for solar hydrogen production. Part I: Decomposition of sulfuric acid", *Solar Energy*, Vol. 78, pp. 632-646, 2005.

[25] W. Xinxin, O. Kaoru, "Thermochemical water splitting for hydrogen production utilizing nuclear heat from an HTGR", *Tsinghua Science and Technology*, Vol. 10, pp. 270-276, 2005.

[26] R. Liberatore, M. Lanchi, A. Giaconia, P. Tarquini, "Energy and economic assessment of an industrial plant for the hydrogen production by water-splitting through the sulfur-iodine thermochemical cycle powered by concentrated solar energy", *International Journal of Hydrogen Energy*, Vol. 37, 9550-9565, 2012.

[27] F. Varsano, M. A. Murmura, B. Brunetti, F. Padella, A. La Barbera, C. Alvani, M. C. Annesini "Hydrogen production by water splitting on manganese ferrite-sodium carbonate mixture: Feasibility tests in a packed bed solar reactor-receiver", *International Journal of Hydrogen Energy*, Vol. 39, pp. 20920-20929, 2014.

[28] C. Canavesio, H. E. Nassini, A. E. Bohe "Evaluation of an iron-chlorine thermochemical cycle for hydrogen production", *International Journal of Hydrogen Energy*, Vol. 40, pp. 8620-8632, 2015.

[29] R. Xu, T. F. Wiesner "Conceptual design of a two-step solar hydrogen thermochemical cycle with thermal storage in a reaction intermediate", *International Journal of Hydrogen Energy*, Vol. 39, pp. 12457-12471, 2014.

[30] M. A. Lewis, J. G. Masin, P. A. O'Hare, "Evaluation of alternative thermochemical cycles, Part I: The methodology", *International Journal of Hydrogen Energy*, Vol. 34, pp. 4115-4124, 2009.

[31] M. A. Lewis, J. G. Masin, "The evaluation of alternative thermochemical cycles – Part II: The down-selection process", *International Journal of Hydrogen Energy*, Vol. 34, pp. 4125-4135, 2009.

425   [32] M. A. Lewis, M. S. Ferrandon, D. F. Tatterson, P. Mathias, "Evaluation of alternative thermochemical

426   cycles – Part III further development of the Cu-Cl cycle", *International Journal of Hydrogen Energy*, Vol.

427   34, pp. 4136-4145, 2009.

428   [33] I. Dincer, M. T. Balta, "Potential thermochemical and hybrid cycles for nuclear-based hydrogen

429   production", *International Journal of Energy Research*, Vol. 35, pp. 123-137, 2011.

430   [34] Z. L. Wang, G. F. Naterer, K. S. Gabriel, R. Gravelsins, V. N. Daggupati, "Comparison of different

431   copper-chlorine thermochemical cycles for hydrogen production", *International Journal of Hydrogen

432   Energy*, Vol. 34, pp. 3267-3276, 2009.

433   [35] M. Serban, M. A. Lewis, J. K. Basco, "Kinetic study of the hydrogen and oxygen production reactions

434   in the copper-chloride thermochemical cycle", AIChE 2004 Spring National Meeting, New Orleans, LA,

435   2004.

436   [36] G. F. Naterer, S. Suppiah, M. Lewis, K. Gabriel, I. Dincer, M. A. Rosen, M. Fowler, G. Rizvi, E. B.

437   Easton, B. M. Ikeda, M. H. Kaye, L. Lu, I. Pioro, P. Spekkens, P. Tremaine, J. Mostaghimi, A. Avsec, J.

438   Jiang, "Recent Canadian advances in nuclear-based hydrogen production and the thermochemical Cu-Cl

439   cycle", *International Journal of Hydrogen Energy*, Vol. 34, pp. 2901-2917, 2009.

440   [37] G. F. Naterer, S. Suppiah, L. Stolberg, M. Lewis, M. Ferrandon, Z. Wang, I. Dincer, K. Gabriel, M.

441   A. Rosen, E. Secnik, E. B. Easton, L. Trevani, I. Pioro, P. Tremaine, S. Lvov, J. Jiang, "Canada's program

442   on nuclear hydrogen production and the thermochemical Cu-Cl cycle.", *International Journal of Hydrogen

443   Energy*, Vol. 36, pp. 15472-15485, 2011.

444   [38] G. F. Naterer, S. Suppiah, L. Stolberg, M. Lewis, M. Ferrandon, Z. Wang, I. Dincer, K. Gabriel, M.

445   A. Rosen, E. Secnik, E. B. Easton, L. Trevani, I. Pioro, P. Tremaine, S. Lvov, J. Jiang, "Clean hydrogen

446   production with the Cu-Cl cycle – Progress of international consortium, I: Experimental unit operations",

447   *International Journal of Hydrogen Energy*, Vol. 36, pp. 15486-15501, 2011.

448   [39] G. F. Naterer, S. Suppiah, L. Stolberg, M. Lewis, M. Ferrandon, Z. Wang, I. Dincer, K. Gabriel, M.

449   A. Rosen, E. Secnik, E. B. Easton, L. Trevani, I. Pioro, P. Tremaine, S. Lvov, J. Jiang, "Clean hydrogen

production with the Cu-Cl cycle – Progress of international consortium, II: Simulations, thermochemical data and materials", *International Journal of Hydrogen Energy*, Vol. 36, pp. 15486-15501, 2011.

[40] C. Zamfirescu, I. Dincer, G. F. Naterer, "Thermophysical properties of copper compounds in the copper-chlorine thermochemical water splitting cycles", *International Journal of Hydrogen Energy*, Vol. 35, pp. 4839-4852, 2010.

[41] A. Ozbilen, I. Dincer, M. A. Rosen, "Environmental evaluation of hydrogen production via thermochemical water splitting using the Cu-Cl cycle: A parametric study, *International Journal of Hydrogen Energy*, Vol. 36, pp. 9514-9528, 2011.

[42] M. S. Ferrandon, M. A. Lewis, D. F. Tatterson, A. Gross, D. Doizi, L. Croize, V. Dauvois, J. L. Roujou, Y. Zanella, P. Carles, "Hydrogen production by a Cu-Cl thermochemical cycle: Investigation of the key step of hydrolysing $CuCl_2$ to Cu_2OCl_2 and HCl using a spray reactor", *International Journal of Hydrogen Energy*, Vol. 35, pp. 992-1000, 2010.

[43] G. F. Naterer, V. N. Daggupati, G. Marin, K. S. Gabriel, Z. L. Wang, "Thermochemical hydrogen production with a copper-chlorine cycle, II: Flashing and drying of aqueous cupric chloride", *International Journal of Hydrogen Energy*, Vol. 33, pp. 5451-5459, 2008.

[44] G. F. Naterer, K. Gabriel, Z. L. Wang, V. N. Daggupati, R. Gravelsins, "Thermochemical hydrogen production with a copper-chlorine cycle. I: Oxygen release from copper oxychloride decomposition", *International Journal of Hydrogen Energy*, Vol. 33, pp. 5439-5450, 2008.

[45] S. Ghandehariun, M. A. Rosen, G. F. Naterer, Z. Wang, "Pinch analysis for recycling thermal energy in the Cu-Cl cycle", *International Journal of Hydrogen Energy*, Vol. 37, pp. 16535-16541, 2012.

[46] S. Ghandehariun, M. A. Rosen, G. F. Naterer, Z. Wang, "Comparison of molten salt heat recovery options in the Cu-Cl cycle of hydrogen production", *International Journal of Hydrogen Energy*, Vol. 36, pp. 11328-11337, 2011.

[47] S. Ghandehariun, G. F. Naterer, M. A. Rosen, Z. Wang, "Indirect contact heat recovery with solidification in thermochemical hydrogen production", *Energy Conversion and Management*, Vol. 82, pp. 212-218, 2014.

476   [48] R. Clift, M. E. Weber, J. R. Grace, Bubbles, drops, and particles, Academic Press, N.Y., 1978.

477   [49] W. Ranz, W. Marshall, "Evaporation from drops", *Chemical Engineering Progress*, Vol. 48, pp. 141-

478   146, 1952.

479   [50] B. D. Cullity, Elements of x-ray diffraction, Addison-wesley Publishing Company, Massachusetts,

480   1956.

481   [51] S. J. Kline, F. A. McClintock, "Describing uncertainties in single-sample experiments", *Mechanical*

482   *Engineering*, Vol. 75, pp. 3-8, 1953.

483

484

485   Table 1. Technical specifications of Optris PI160

Detector	FPA, uncooled
Spectral range	7.5-13 µm
Optical resolution	160×120
Frame rate	120 Hz
Temperature range	150-900ºC
Accuracy	±2ºC or ±2%

486

487

488

489   Table 2. Technical specifications of Flir Sc5600

Sensor type	InSb
Waveband	3-5 µm
Pixel resolution	640×512
Pitch	15 µm
Cooler	Close cycle Stirling cooler
Maximum frame rate (full frame)	100 Hz
Integration time	200 ns to 20 ms
Temperature measurement range	5 -1500ºC
Temperature measurement accuracy	±1ºC or ±1%

490

491

492

493

22

494

495

496

497

498
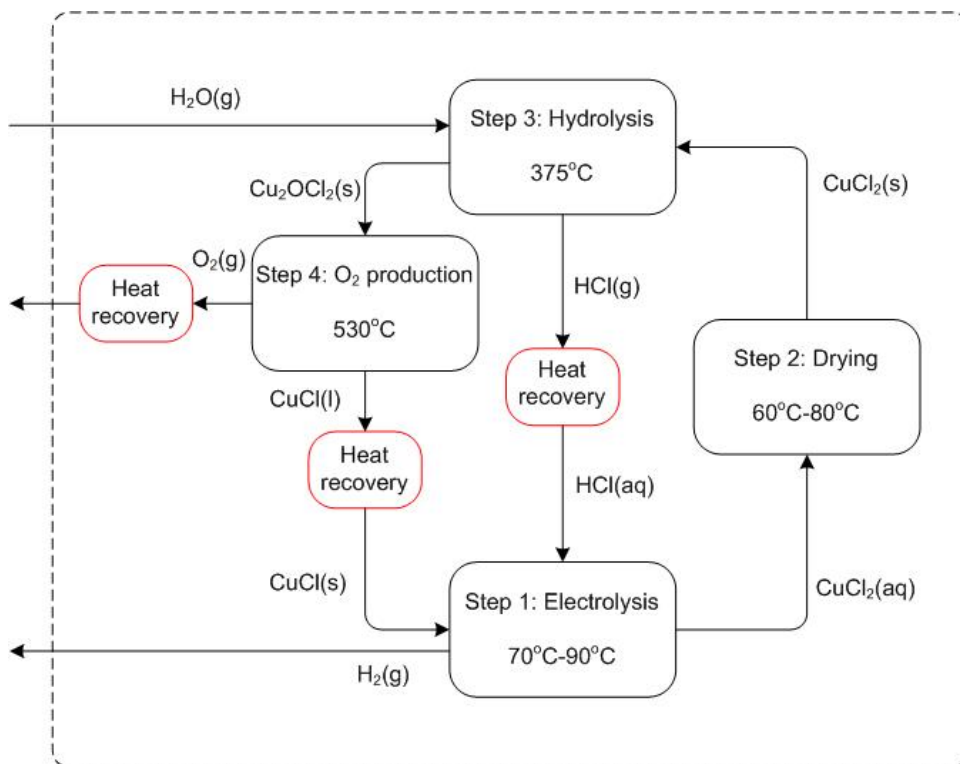
Fig. 1 Schematic of the four step copper-chlorine cycle for thermochemical water splitting

499

500

501

502
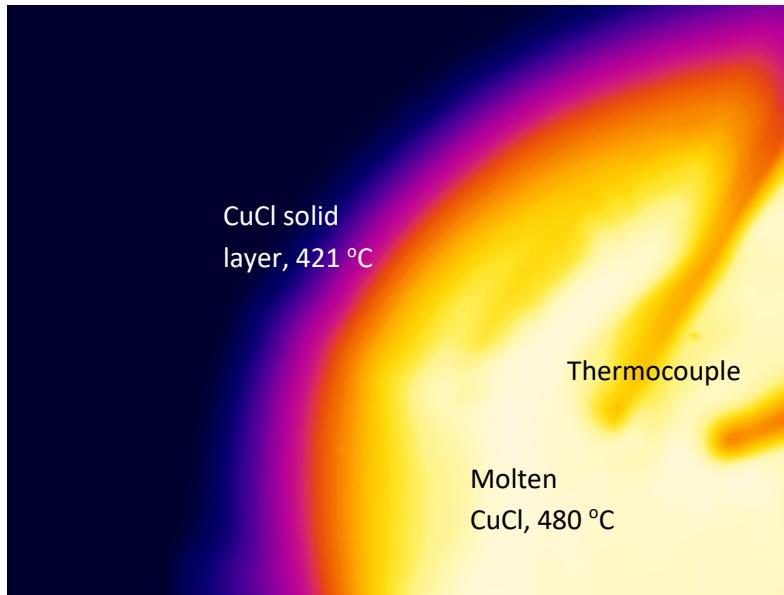
Fig. 2 Temperature measurement of CuCl using Optris PI160 thermal imager

503

504

505

506

507

508

Fig. 3 Thermal image of molten CuCl droplets at the exit of an inclined tube

509

510

511

512

24
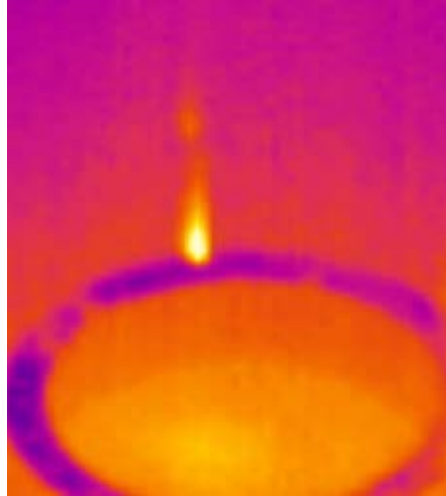
513

514   Fig. 4 Thermal image of a falling droplet generated with an inclined tube using Optris PI160

515

516

517

518

519

520

521
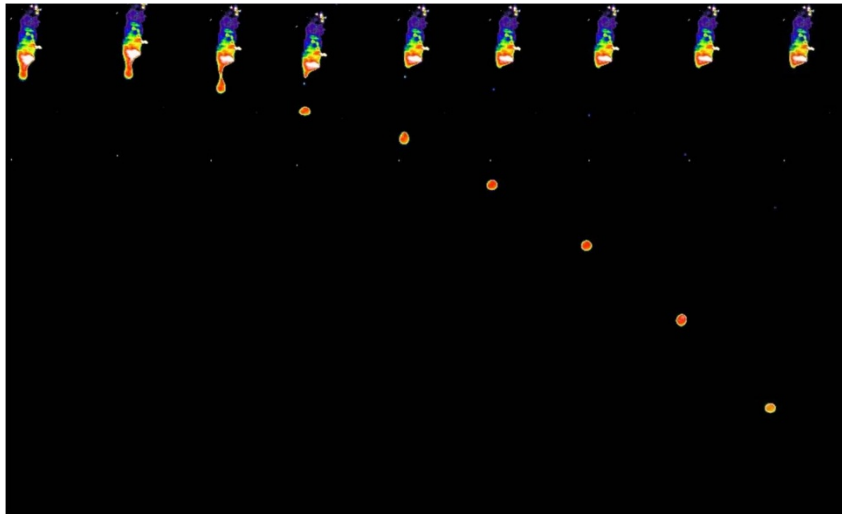
522

523   Fig. 5 Thermal image of molten CuCl droplets in descent using FLIR SC5600

524
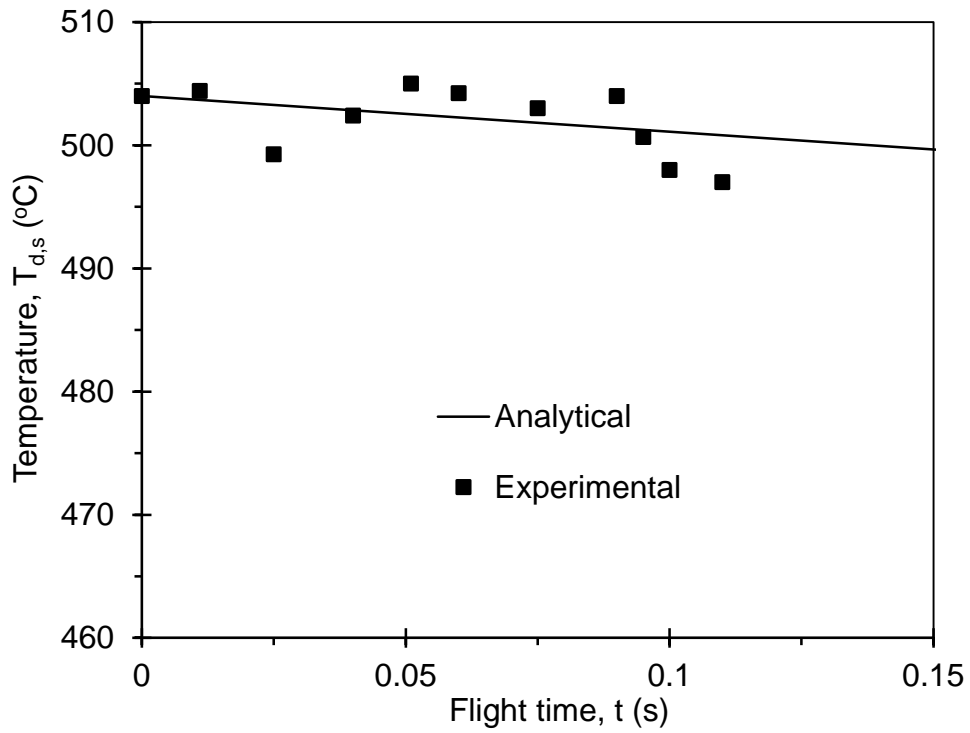
Fig. 6 Droplet temperature versus flight time

(a) CuCl molten droplet hits the water surface and forms a steam bubble

(b) CuCl droplet leaves the water surface

26

534

535   (c) Steam bubble breaks to release steam

536

537   (d) Droplet breaks into many flakes

538   Fig. 7 Quenching of a droplet in water

539

540

541

542

543

544   Fig. 8 CuCl droplets break into many small flakes

545

546

547

548

549   Fig. 9 Solidified CuCl from the water vessel

550
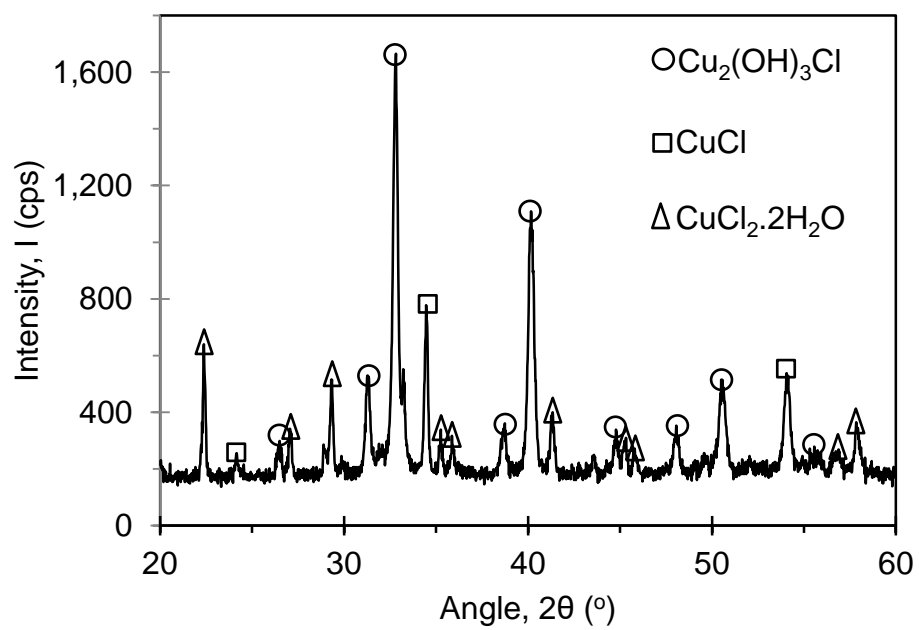
551

552   Fig. 10 X-ray diffraction results for CuCl in contact with air and water
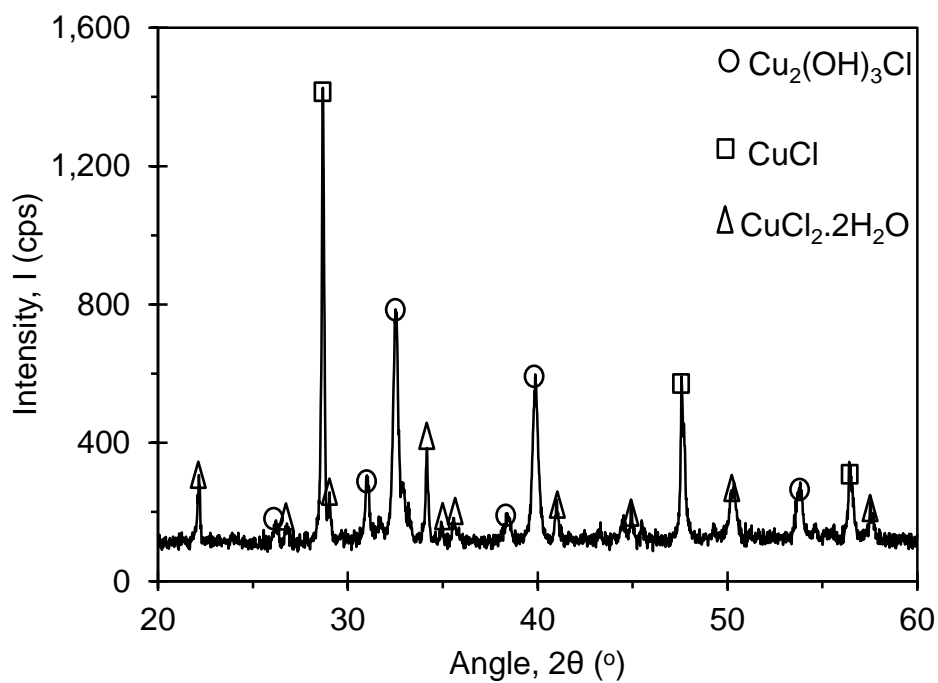
553

554   Fig. 11 X-ray diffraction results for CuCl in contact with air and water

555

556
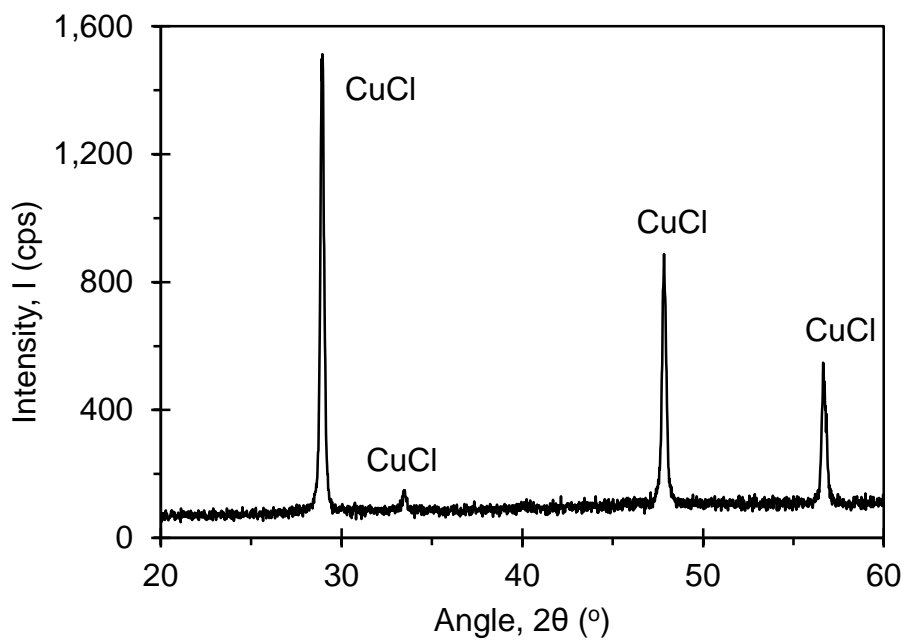
557

558   Fig. 12 X-ray diffraction results for CuCl in contact with water

559
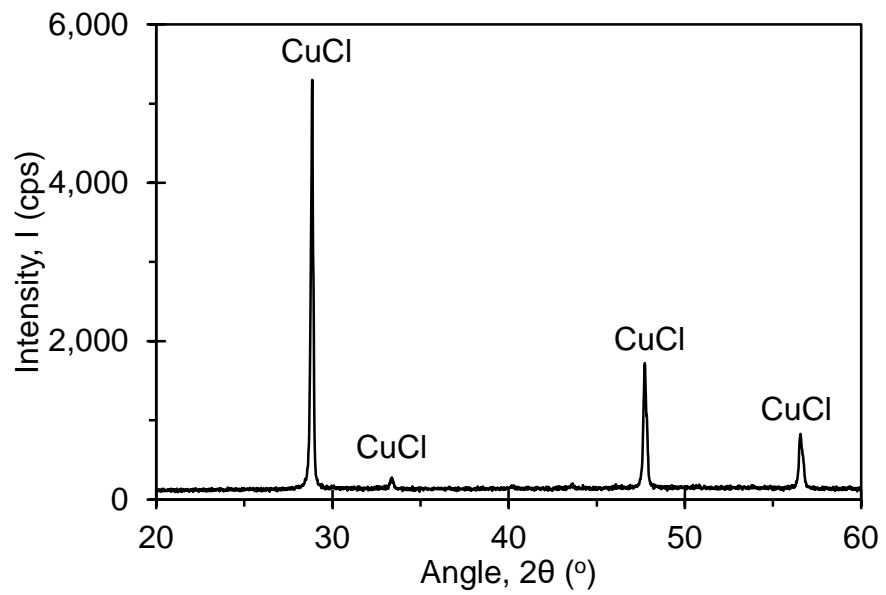
560

561   Fig. 13 X-ray diffraction results for CuCl in contact with water